Journal of Trace Elements in Medicine and Biology 80 (2023) 127302

Contents lists available at ScienceDirect

Journal of Trace Elements in Medicine and Biology

journal homepage: www.elsevier.com/locate/jtemb

Iron oxide nanoparticles induced cytotoxicity, oxidative stress, cell cycle arrest, and DNA damage in human umbilical vein endothelial cells

Maqsood A. Siddiqui [a,*,1], Rizwan Wahab [a], Quaiser Saquib [a], Javed Ahmad [a], Nida N. Farshori [b], Ebtesam S. Al-Sheddi [b], Mai M. Al-Oqail [b], Shaza M. Al-Massarani [b], Abdulaziz A. Al-Khedhairy [a]

[a] Chair for DNA Research, Zoology Department, College of Science, King Saud University, P.O. Box 2455, Riyadh 11451, Saudi Arabia
[b] Department of Pharmacognosy, College of Pharmacy, King Saud University, P.O. Box 22452, Riyadh 11495, Saudi Arabia

ARTICLE INFO

Keywords:
Iron oxide nanoparticles
Cytotoxicity
Oxidative stress
DNA Damage
Cell cycle arrest
Gene expression

ABSTRACT

Background: Nanotechnology and material science have developed enormously fast in recent years. Due to their excellent magnetic properties, iron oxide nanoparticles (IONPs) have been broadly applied in the field of bioengineering and biomedical. Thus, it is important to evaluate the safety issues and health effects of these nanomaterials. The present investigation was aimed to evaluate the adverse effects of IONPs on human umbilical vein endothelial cells (HUVECs).

Methods: The cytotoxic potential of IONPs was assessed by MTT and neutral red uptake (NRU) assays. The impact of IONPs on oxidative stress markers (glutathione (GSH) and lipid peroxidation (LPO)), reactive oxygen species (ROS) production, and mitochondrial membrane potential (MMP) was also examined. Furthermore, the toxic effect of IONPs was quantified by assessing DNA damage, cell cycle arrest, and apoptosis by quantitative real time PCR.

Results: We found that IONPs induce a dose-dependent cytotoxicity on HUVECs with IC_{50} value of 79.13 μg/mL. The results also displayed that IONPs induce oxidative stress, ROS production, and mitochondrial membrane dysfunction. The comet assay results exhibited IONPs induces DNA damage in HUVECs. We found significant cell cycle arrest at SubG1 phase in treated cells and consequent cell death was evidenced by microscopic analysis. Moreover, IONPs display substantial up-regulation of pro-apoptotic genes and down-regulation of anti-apoptotic gene evidenced by real time qPCR.

Conclusion: Overall, our results clearly demonstrated that IONPs have the potential to induce cytotoxicity, DNA damage, cell cycle arrest, and apoptosis in HUVECs mediated through oxidative stress and ROS production. Thus, IONPs are cytotoxic and it should be handled with proper care.

1. Introduction

Nanotechnology is a fast-growing field and become one of the most developing areas of the science and technology worldwide [1]. Nanotechnology includes engineering, synthesis, and utilization of nanomaterials, which are chemical molecules smaller than 100 nm with unique physicochemical characteristics [2]. The novel physiochemical and biological properties of these nanomaterials make them valuable in several products for humans, such as cosmetics, electronics, agriculture, clothing, food, medicine, and other industrial business [3,4]. It is documented that nanotechnology growth, exploration, and manufacturing have been intensely rising and projected that nanoproducts will contribute to worldwide economy [5]. Consequently, human being may be exposed to nanomaterials through skin contact, respiratory pathways, blood circulation, and ingestion [6]. Due to their small size and high surface ratio, nanoparticles can easily pass via cell membrane and other biological fences, hence they can effortlessly accumulate into active organisms and induces cellular damages [7,8]. Furthermore, researches concerning the cellular toxicity of these nanoparticles are desired for the harmless use [9]. Numerous manufactured metal and metal oxide nanoparticles with commercial and industrial applications, are presented into everyday life, such as paints, sunscreen, cosmetics, pigments, plastics, ceramic products, coatings, food additives, personal care products, and drug delivery agents [10,11]. The

* Corresponding author.
E-mail addresses: maqsoodahmads@gmail.com, masiddiqui@ksu.edu.sa (M.A. Siddiqui).
[1] *(ORCID: 0000–0002-2010–3088)*

https://doi.org/10.1016/j.jtemb.2023.127302
Received 24 June 2023; Received in revised form 21 August 2023; Accepted 6 September 2023
Available online 7 September 2023
0946-672X/© 2023 Elsevier GmbH. All rights reserved.

increasing application of these nanoparticles has elevated serious concern about their possible adverse effect on human health [12]. Thus, the understanding the connections of nanoparticles with biological systems is an utmost important scientific matter. The toxicity of various metal and metal oxide nanoparticles such as silver, gold, copper, aluminum, titanium, zinc, iron, nickel, cobalt etc. have been broadly studied under different biological systems using in vitro and in vivo models [13–15]. Even though several investigations have established diverse toxic effects related to nanoparticles, such as oxidative stress, changed cell cycle regulation, mitochondrial damage, protein denaturation, and DNA damage [16]. Still, very little is known about underlying mechanisms answerable for the toxic effects of nanoparticles. An important mechanism of these nanoparticles is ROS generation, resulting in the successive development of oxidative damage in cells, thus activating inflammatory responses [5]. Oxidative stress and inflammation are accountable for damaging molecules, such as proteins, DNA, and lipids, hence causing tissue/cell damage which can conclude in cytotoxicity and genotoxicity [17]. The different nanoparticles exhibit different toxic effects [18]. Among the various nanoparticles, IONPs have been considered in several biomedical fields for magnetic resonance imaging contrast, intravenous cell targeting, separation and labelling, drug delivery system, and therapeutic uses of hyperthermia [19,20]. The features characteristic to nanosystem including IONPs incline to directly affect with their toxicity. For example, the changes in shape and size of the IONPs were revealed to play a significant part on cell toxicity [21]. It is also reported that surface charge of IONPs could produce genotoxicity and cytotoxicity. The positively charged IONPs were shown to be more toxic as they endure non-specific communication and adsorptive endocytosis with negatively charged cell membrane, consequently cumulative the intracellular accumulation and disturbing the integrity of cell membrane [22]. The cytotoxicity of IONPs is moderately elucidated by ROS generation which leads cellular oxidative stress. Oxidative stress is the eminent cause of cell damage and toxicity, the exposure to IONPs can also produce deleterious effects and leads to cell death [23]. Several investigators have examined the cytotoxic potential of IONPs on various type of cells [24,25], still their potential toxicity upon endothelium is not well known. Since, blood vessel is one of the main barriers for IONPs application to diagnosis and therapeutics, therefore potential effects of IONPs on human vascular endothelial cells needs to be explored in details. Although it is reported that IONPs exposure induced cytotoxicity and morphological alteration on endothelial cells [26,27]. However, the mechanism underlying the toxicity of IONPs have not been widely studied till now. One of the key reasons for the nonexistence of information on the mechanism of actions of IONPs, is that the comprehensive toxicity studies have not been conducted. Thus, in present work, we have studied the systematic toxic effects of IONPs on HUVECs and underlying mechanism of IONPs induced cell death.

2. Materials and methods

2.1. Synthesis of IONPs

IONPs were formed using iron nitrate nonahydrate ($Fe(NO_3)_3.9\ H_2O$; Sigma) and sodium hydroxide (NaOH; Sigma) [28]. Briefly, $Fe(NO_3)_3.9\ H_2O$ (0.035 M) was dissolved in 100 mL double distilled water with constant stirring at the speed of 800 rpm. Once the clear brown color solution was obtained, NaOH (0.01 M; 100 mL), was added in this solution slowly and mix well. The obtained solution pH was checked via pH meter (Cole Parmer, U.S.A) and it touched to 12.35. Then solution was moved to refluxing pot and heated at ~80 °C for 1 h. After the end of reaction, the glass pot was stored at a cool place for 24 h. Thereafter, the semi aqueous product was centrifuged at 3000 rpm for 5 min via centrifugation. The product was further washed with alcohol and dried at room temperature for further analysis.

2.2. Characterizations

The X-ray diffraction pattern powder (XRD) was utilized for the observation of the prepared powder material. The $Cu_{K\alpha}$ radiation (λ = 1.54178 Å) source was used with angle rotation ranging from 10° to 80° with 6°/min scanning speed. The morphology of the prepared nanostructure powder was examined via scanning electron microscopy (SEM) at room temperature. For this, the powder was uniformly dispersed on carbon tape, pasted on sample holder. The sample holder was coated with powder and transferred it to sputtering chamber for ~2–3 *s* to get the conducting layer on the surface of powder sample. Once the sputtering was completed, sample holder was fixed to the SEM and analyzed. To get more clarification, the powder sample was further investigated via transmission electron microscopy (TEM, JEOL JEM-1011, Japan at 200 kV). For the observation, a pinch of synthesized powder was sonicated for ~10–15 min in an ethanol (EtOH) solvent with a 50 mL capacity beaker. Once the sonication was completed, a copper grid (400 mesh size) was inserted to this solution for ~2–3 *s* and removed from the suspension solution and dried it at room temperature. The grid was fixed in a sample holder and analyzed the sample at room temperature [29]. The Fourier transform infrared (FTIR, Perkin Elmer's GX spectrophotometer, U.S.A) spectroscopy was analyzed in the range of 400–4000 cm^{-1}. The thermal stability test in terms of thermal gravimetric analysis (TGA) instrument (Mettler Toledo AG, Analytical CH-8603, Schwerzenbach, Switzerland) was conducted for the analysis of prepared product. For this experiment ~11.5 mg of powder was loaded into alumina crucibles (Al_2O_3) and heated till to 900 °C with a heating ramp of 20 °C/min under nitrogen gas with a flow of 20 mL/min. The hydrodynamic size and zeta potential of IONPs were also measured. For this, the IONPs were suspended in deionized water and sonicated. The hydrodynamic size and zeta potential of IONPs in aqueous suspension were analyzed using a dynamic light scattering (DLS) (Zetasizer, Nano-ZS, Malvern, UK).

2.3. Cell culture

HUVECs (CRL-1730) obtained from American Type Culture Collection (ATCC), Manassas, were grown in Dulbecco's modified Eagle's medium (DMEM; Sigma) complemented with 10% fetal bovine serum (FBS), and 1% antibiotic/antimycotic solution (10,000 units/mL of penicillin, 10,000 μg/mL of streptomycin, and 25 μg/mL of amphotericin B; Gibco, USA). HUVECs were frequently passaged using 0.25% trypsin (Sigma, USA).

2.4. Exposure to IONPs

The HUVECs were harvested using trypsin and seeded in 25 cm^2 flasks, 96-, 48-, and 24-well plates according to the experimental requirements. A stock solution of IONPs (10 mg/mL) was prepared in phosphate buffer saline (PBS) and diluted to appropriate concentrations for the exposure. The control groups (culture medium only) were run parallel in each assay.

2.5. Cytotoxicity (MTT) assay

MTT assay for IONPs in HUVECs was conducted as per the method defined [30]. HUVECs were counted, and plated in a 96 well plate at a density of 10000 cells/well. Then exposed to IONPs concentrations ranging from 5 μg/mL to 100 μg/mL. After 24 h of exposure, 10 μL (5 mg/mL) of MTT (3-[4,5-dimethylthiazol-2-yl]−2,5-diphenyltertrazolium bromide) was added to wells. Then after 4 h incubation at 37ºC, the solution was aspirated and 200 μL of dimethyl sulfoxide (DMSO) was added to wells and mixed gently. The developed color was measured at 550 nm.

2.6. Neutral red cytotoxicity assay

HUVECs (10000 cells/well) plated in a 96 well, were incubated for 24 h to grow [31]. The media was then replaced with IONPs (5 μg/mL to 100 μg/mL). Following the 24 h incubation, 100 μL of serum free media comprising neutral red (50 μg/mL) was added to each well. After 3 h incubation, the cells were washed with washing buffer (1% $CaCl_2$ and 1% formaldehyde) subsequently 200 μL of dye extraction solution (1% acetic acid and 50% ethanol) was added to wells and mixed well. The absorbance was measured at 550 nm.

2.7. Observation of morphological changes

To observe the changes induced by IONPs, HUVECs were exposed to IONPs (5 μg/mL to 100 μg/mL) for 24 h. Afterward, cells were visualized directly under the light microscope (CKX41; Olympus, Japan) at 20 × magnification.

2.8. Estimation of GSH

GSH level in HUVECs was measured by the procedure of Chandra et al. [32]. Briefly, HUVECs exposed to 60–100 μg/mL of IONPs, were harvested and sonicated. The supernatant was then mixed with 10% trichloroacetic acid (TCA) for precipitation. After centrifugation, to 2 mL of supernatant, 2 mL of 0.4 M tris buffer containing 0.04 M of ethylenediaminetetraacetic acid (EDTA) and 0.01 M of 5,5-dithio-bis-(2-nitrobenzoic acid) (DTNB) was mixed and incubated at 37°C for 10 min. Then developed color was measured at 420 nm.

2.9. Estimation of LPO

LPO level in HUVECs treated with 60 μg/mL, 80 μg/mL, and 100 μg/mL of IONPs was estimated by TBARS (Thiobarbituric acid reactive substances) method [33]. Post 24 h exposure, cells were collected in 1.15% KCl buffer. After sonication, 2 mL of thiobarbaric acid (TBA) reagent (15% TCA, 0.7% TBA, and 0.25 N HCl) was added into supernatant. The solution was boiled for 15 min, centrifuged, and developed color was read at 532 nm.

2.10. Measurement of ROS generation

ROS generation induced by IONPs was quantified using a cell permeable fluorescent dye (2,7-dichlorodihydrofluorescein diacetate; DCFDA) [34]. HUVECs were grown in a 24-well plate. Then, culture medium was aspirated and IONPs with varying concentrations (60 μg/mL, 80 μg/mL, and 100 μg/mL) were added in medium and exposed for 24 h. Further medium was changed with freshly prepared medium containing DCFDA and incubated at 37°C for 1 h. Cells were then washed and imagined on fluorescence microscope. In a parallel set of experiment, the fluorescence intensity of DCF in HUVECs treated with IONPs was measured using fluorescence reader (Fluoroskan Ascent, Thermo Scientific, Finland) with a 485 nm for excitation and 538 nm for emission wavelengths.

2.11. MMP level analysis

The fluorescent probe dye Rhodamine-123 (Rh-123) was used to assess MMP level of HUVECs post IONPs exposure. Briefly, HUVECs were cultured in a 24-well plate at a density of 2×10^4 cells/well. After overnight incubation, cells were exposed to IONPs (60 μg/mL, 80 μg/mL, and 100 μg/mL) for 24 h. Following IONPs exposure, solution was discarded and Rh-123 dye was added to cells. After 60 min incubation at 37°C in absence of light, cells were washed and fluorescence intensity was imagined on fluorescence microscope. In a separate set of experiment, the fluorescence intensity of Rh-123 in IONPs treated HUVECs was measured using 485 nm for emission and 528 nm for excitation wavelengths.

2.12. Cell cycle assay

The HUVECs were cultured in 24-well at a density of 2×10^4 cells/well. After overnight culture, cells were exposed to IONPs at 60, 80, and 100 μg/mL for 24 h. The cells were subsequently fixed with 70% ethanol for 60 min and stained with propidium iodide (PI) for 30 min. The cell populations under different cell cycle phases were counted by employing 10,000 cells in a flow cytometry (Coulter counter, USA).

2.13. Comet assay (DNA damage)

The conventional comet assay was done in alkaline conditions as designated earlier [35]. In brief, the HUVECs were seeded in a 24-well plate and exposed to IONPs (60–100 μg/mL) for 24 h. After the exposure, cells were collected and followed the remaining steps as mentioned in the conventional comet assay method. Nearly, 100 cells/slide were independently counted under Nikon i80 fluorescence microscope (Nikon, USA). The comet software (Comet assay IV, Perceptive Instruments, UK) was used to estimate the mean value of percentage DNA in olive tail moment.

2.14. Quantitative real time PCR

To ascertain the role of apoptotic marker genes in HUVECs treated with IONPs, gene expression profile of apoptotic related genes was evaluated by quantitative real time PCR [36]. In brief, HUVECs were seeded in 6-well plate, incubated overnight and exposed to 100 μg/mL of IONPs. Then, total RNA was extracted from treated and untreated groups using RNeasy mini kit (Qiagen) as per the instruction provided with kit. Purity of RNA was analyzed by Nanodrop 8000 (Thermo scientific, USA). Further using 2 μg of total RNA, cDNA was performed by using MLV reverse transcriptase kit (GE Healthcare, UK). The cDNA was mixed with master mix (100 ng of cDNA, 7.5 μM respective primers, and 2x of CYBR Green I) for the preparation of qPCR. The plates containing all reagents were centrifuged and qPCR was completed on Roche® LightCycler®480 detector (96 well format) under following conditions: 95 °C for 10 min, 40 cycles of 95 °C for 15 s, 60 °C for 20 s, and 72 °C for 20 s. The obtained threshold cycle values were regularized to the GAPDH gene. The expression of apoptotic genes was presented as fold ratio values. The sequences of primers used for qPCR are as: p53 (F) 5′-CCCAGCCAAAGAAGAAACCA-3′, (R) 5′-TTCCAAGGCCTCATTCAGCT-3′; bax (F) 5′-TGCTTCAGGGTTTCATCCAG-3′, (R) 5′-GGCGGCAATCATCCTCTG-3′; caspase-3 (F) 5′-ACATGGCGTGTCATAAAATACC-3′, (R) 5′-CACAAAGCGACTGGATGAAC-3′; caspase-9 (F) 5′-CCAGAGATTCGCAAACCAGAGG-3′, (R) 5′-GAGCACCGACATCACCAAATCC-3′; bcl-2 (F) 5′-AGGAAGTGAACATTTCGGTGAC-3′, (R) 5′-GCTCAGTTCCAGGACCAGGC-3′; GAPDH (F) 5′-CCACTCCTCCACCTTTGAC-3′, (R) 5′-ACCCTGTTGCTGTAGCCA-3′.

2.15. Statistical examination

The data are presented as mean ± S.D. To detect statistically significant changes among control and treated groups, one-way ANOVA and Dunnett's multiple compression test was employed. p values < 0.05 was interpreted as statistically significant.

3. Results

3.1. X-ray diffraction pattern of IONPs

The XRD pattern illustrates the phase, size, and crystallinity of the prepared powder. From the obtained observation, it expresses that the

material is iron oxide and fully analogous to the accessible phase identification JCPDS cards no. 39–1346. The peak positions such as 23.95 <012>, 32.95 <104>, 35.45<110>, 40.60 <113>, 49.35 <024>, 53.90 <11 6>, 57.4 <018>, 62.3 <214>, 63.85 <300>, 71.75 <1010 > and 75.35 <220> clearly coincides with iron oxide (Fig. 1). The estimated crystallite size of an individual NPs is ~13 ± 1 nm calculated by Scherrer formula. The diffraction spectrum doesn't show any other peak which indicates that the prepared material is pure and free from any hydroxide or organic material.

3.2. Morphology of the prepared product (SEM and TEM)

The structural morphology was analyzed by SEM and TEM. Fig. 2 A shows the structure of bulk and Fig. 2B, C represents the SEM images of IONPs captured at low and high magnification, respectively. Several very small, fine and densely packed grains were seen in the image (Fig. 2B). The image captured at high magnification discloses that the projected size on an individual particle is about 11 nm. The size distribution was also calculated based on the SEM and results are provided in Fig. 2D. For more detailed observation, the prepared IONPs were further examined via TEM at room temperature. As found in the SEM images, a similar result was also detected in TEM. Very small and fine particles were seen joint together. The estimated size of each individual particle was ~11 nm with spherical shaped morphology (Fig. 3 A). The obtained data observation is in line and fully consistent with the obtained X-ray diffraction and SEM data.

3.3. Fourier transform infrared spectroscopy (FTIR)

The FTIR spectroscopy was utilized to know the functional groups presents in the prepared IONPs. Fig. 3B, illustrates a shallow and broad peak between 3200 and 3600 cm^{-1} corresponding to water molecule (H-O-H). The exact peak position of water molecule was obtained at 3460 cm^{-1}. A sharp, small, and pointed of asymmetric stretching band of hydroxyl (-OH) was obtained at 1642 cm^{-1}. A shallow and small band pinpointed at 1063 cm^{-1} was associated with the stretching mode of nitrate (NO_3^{-1}) group from the iron nitrate. A pointed and long peak observed at 563 cm^{-1} denoted represents metal oxide of iron oxide formation, whereas a pointed and short peak observed at 479 cm^{-1} represent the asymmetric stretching of iron oxide. The obtained FTIR spectroscopy result shows that the prepared powder exhibits good chemical characteristics and analogous to other analyzed data. The absence of any additional peaks in the spectrum, further reveal that the IONPs are pure and free from any other additives.

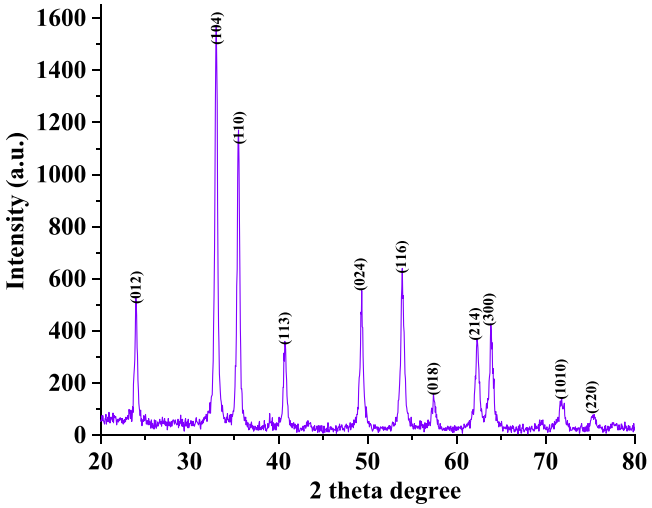

Fig. 1. X-ray diffraction pattern of IONPs.

3.4. Thermogravimetric analysis (TGA)

The thermogravimetric analysis (TGA) is a technique via % mass loss was examined with increasing temperature. The recovered TGA data (Fig. 3 C) express that powder sample exhibits two-step of weight loss, one is solvent evaporation whereas another one is the powder stabilization phase respectively. In this experiment, the initial step is the solvent vaporization phase, starts from 83.33 °C and completed at 400.33 °C with a weight loss of 4.50%. The secondary weight loss starts at 405 °C and knows as the chemical decomposition phase, completed at 800 °C with a total weight loss was 10.44%. This phase shows the stabilization phase of these observation and shows very minute quantity was loosed. In this experiment, it is observed that the total weight loss was calculated from 25 °C to 800 °C was 10.44%. From the obtained observations, reveals that the prepared material is highly stable in nature.

3.5. Hydrodynamic size and zeta potential of IONPs

The DLS was used to examine the hydrodynamic size and zeta potential of IONPs. As presented in Fig. 4 A, the individual particle size of the IONPs in aqueous solution was found to be 81 nm. The obtained results showed that IONPs in aqueous solution have possibility to come closer and form an aggregate. The size of IONPs increases with the interaction of other particles. Zeta potential is used to determine the electrical charges that exist on material surfaces. We found that IONPs display the zeta potential value of − 12.20 mV (Fig. 4B), which shows that the particles are stable in aqueous suspension.

3.6. Cytotoxicity of IONPs by MTT assay

The results described in Fig. 5A indicated that IONPs caused a significant decrease in cell viability of HUVECs. We observed that viability of HUVECs was suppressed by up to 91%, 79%, 67%, 49%, and 36% at 20, 40, 60, 80, and 100 μg/mL, respectively, post 24 h exposure of IONPs. The cytotoxic effect of IONPs was observed at 10 μg/mL and higher concentrations of IONPs while maximum effect was observed at 100 μg/mL. Approximately 50% decline in viability of HUVECs was found at ~80 μg/mL of IONPs after 24 h exposure. As Fig. 5A demonstrate, 10 μg/mL and lower concentrations of IONPs did not cause any toxicity to HUVECs. As seen from dose response curve in MTT assay, the IC_{50} value of IONPs in HUVECs was 79.13 μg/mL.

3.7. Cytotoxicity of IONPs by NRU assay

As shown in Fig. 5B, a concentration-dependent cytotoxic effect of IONPs was also noticed in HUVECs cells. The viability of HUVECs was dropped by up to 92%, 80%, 65%, 45%, and 34% at 20, 40, 60, 80, and 100 μg/mL, respectively, post 24 h IONPs treatment. The data show that exposure to IONPs noticeably affect the HUVECs. Similar to MTT assay, no significant cytotoxic effect was detected in HUVECs at 10 μg/mL and lower concentrations.

3.8. Morphological changes in HUVECs

The effect of IONPs was also confirmed by examining the morphological changes in HUVECs. As depicted in Fig. 5C, untreated HUVECs showed no apoptotic features. However, treatment of HUVECs with IONPs exhibited noticeable morphological changes and apoptotic cells with round bodies.

3.9. Effect of IONPs on GSH and LPO levels

Fig. 6 A illustrate the levels of GSH and LPO in IONPs treated HUVECs. The level of GSH was significantly ($p < 0.01$) decreased by up to 13%, 28%, 61% on treatment of IONPs at 60, 80, and 100 μg/mL,

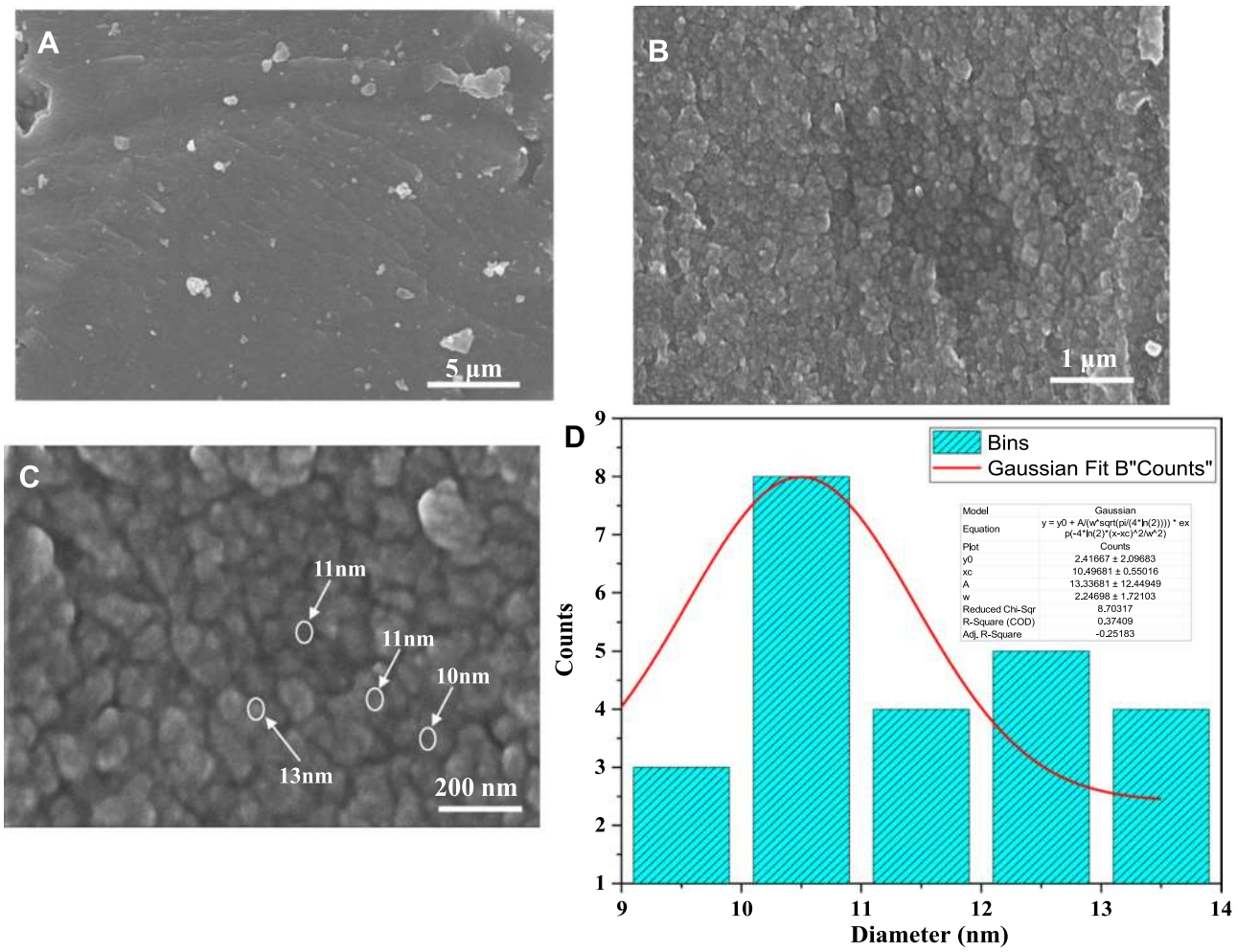

Fig. 2. (A) SEM image of bulk iron oxide nanopowder. Low (B) and high (C) magnification FESEM images of IONPs. (D) Particle size distribution histogram plot determined using SEM images.

respectively. After treatment with IONPs at 60, 80, and 100 µg/mL, the LPO level in HUVECs was also augmented by 121%, 146%, and 180%, respectively when compared with control (Fig. 6A).

3.10. ROS production in IONPs induced HUVECs

The results showed that ROS level in HUVECs following IONPs treatment for 24 h, was significantly increased (Fig. 6B). As shown in Fig. 6B, the fluorescence intensity of DCF was also increased when cells were exposed to 60 µg/mL, 80 µg/mL, and 100 µg/mL of IONPs. Consequently, fluorescence intensity of ROS in IONPs treated HUVECs was also increased by 142%, 184%, and 238% at 60 µg/mL, 80 µg/mL, and 100 µg/mL, respectively compared to control (Fig. 6C).

3.11. Effects of IONPs on MMP

The accretion of ROS in cells can cause oxidative stress which leads to mitochondrial dysfunction. Thus, to quantify the effect of IONPs on MMP, HUVECs were treated with IONPs and stained with Rh-123. As shown in Fig. 7A, a dose dependent decrease in red fluorescence of Rh-123 was noticed following exposure to IONPs. The Rh-123 dye predominates in mitochondria of healthy cells and display a red fluorescence. As evident in Fig. 7B, the fluorescence intensity of Rh-123 was also decreased by 29%, 44%. and 60% at 60, 80, and 100 µg/mL, respectively in IONPs treated HUVCEs.

3.12. DNA damage

The comet assay was conducted to measure the DNA damage induced by IONPs (Fig. 8). We observed that 60–100 µg/mL of IONPs could induce significant DNA damage in HUVECs. Post 24 h exposure to IONPs, percentage olive tail moment (OTM) was augmented in a dose-dependent way. The increase in percentage OTM was observed as 15.6%, 21.9%, and 26.8% at 60, 80, and 100 µg/mL of IONPs, respectively compared to control (0.33%).

3.13. Effect of IONPs on cell cycle arrest

The effect of IONPs on cell cycle progression was estimated by flow cytometry. After 24 h exposure to IONPs significantly inhibited the cell cycle progression in HUVECs. The results are summarized in Fig. 9. After exposure to IONPs, the population of cells in SubG1 phase (indicating apoptotic cells) was dose dependently increased. The proportions of 15.7%, 25.9%, and 48.4% at 60 µg/mL, 80 µg/mL, and 100 µg/mL, respectively was found in SubG1 phase, which were significantly higher compared to untreated control (Fig. 9).

3.14. Expression of apoptotic genes in IONPs treated HUVECs

The expression of apoptotic related genes in IONPs exposed HUVECs was studied using real time qPCR. Exposure to IONPs at 100 µg/mL exhibited upregulation of proapoptotic genes i.e. p53, bax, caspase-3

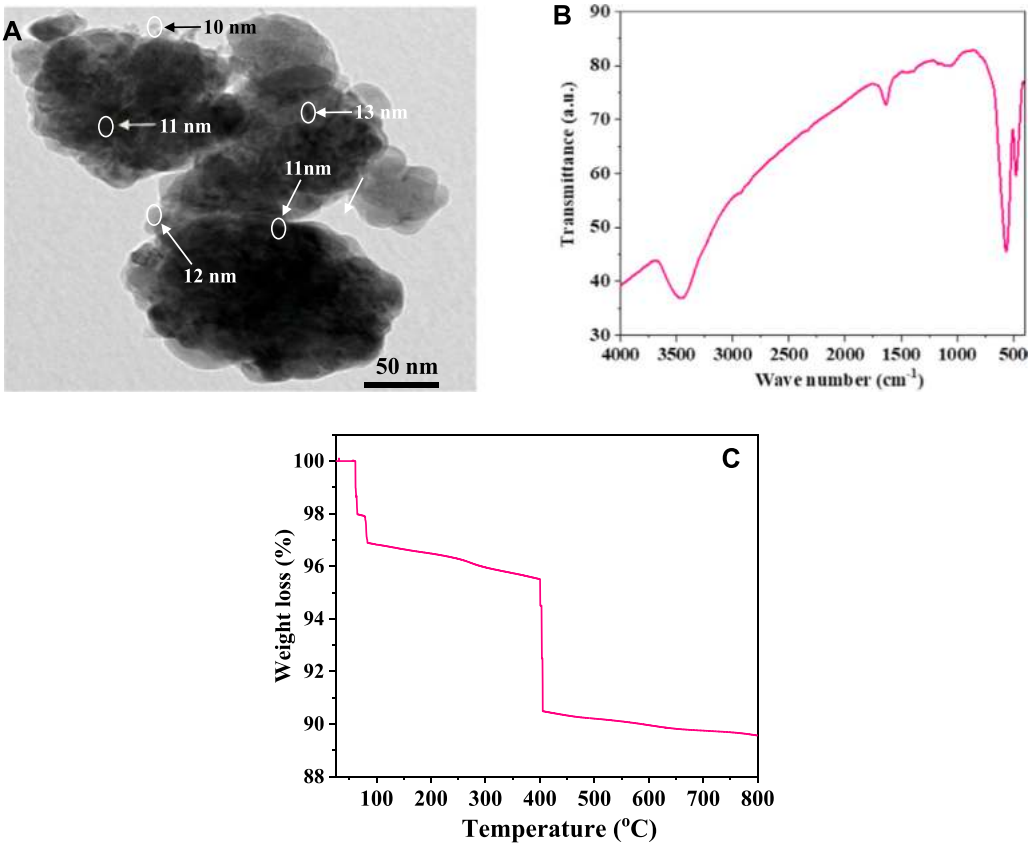

Fig. 3. (A) Shows the TEM, which reveals the general morphology of the NPs in clustered form (average individual size of each nanoparticle is ~11 nm size). (B) Shows the FTIR spectra of IONPs. (C) Thermogravimetric analysis (TGA) of prepared nanoparticles.

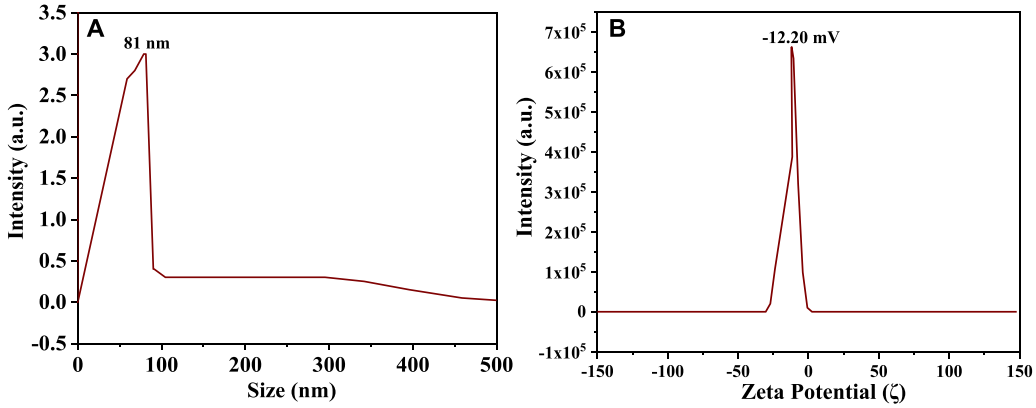

Fig. 4. (A) Shows the hydrodynamic size of IONPs and (B) Displayed the Zeta potential of IONPs.

and − 9 and downregulation of antiapoptotic gene bcl-2 in HUVECs. We observed an upregulation of p53, bax, caspse-3 and − 9 genes by up to 3.1-fold, 2.9-fold, 2.5-fold, and 2.7-fold, respectively, while bcl-2 was downregulated by up to 0.5-fold (Fig. 10).

4. Discussion

IONPs grasp countless potential for utilization in a number of biomedical applications, such as therapeutic agent delivery, diagnosis, and imaging [37]. Irrespective of several advantages, the growing potential applications of IONPs increase concerns about their possible effects on human health. Consequently, it is urgently needed to investigate the toxic potential of IONPs on human health. Previous studies have exposed that IONPs are cytotoxic to certain cells [38]. Endothelial cells line the luminal surface of blood vessels to regulate the blood fluidity. Human umbilical vein endothelial cells (HUVECs) are an important target of nanoparticles when it comes in to the interaction with blood. Hence, present study was designed to explore the toxic effects of IONPs on HUVECs and the mechanism(s) of cell death induced by IONPs.

The physio-chemical description of nanoparticles is important in nanotoxicology as it helps in better understanding of results [5]. The morphological analysis and size of the IONPs was measured by utilizing the SEM/TEM and XRD techniques, respectively. The agglomeration of the particles depends upon several factors such as concentrations of the material, temperature of refluxing pot, and heating time. These parameters revealed that IONPs were spherical, crystalline in nature with an average size of ~11 nm. The functional group of IONPs was also confirmed with FTIR analysis. We also found that IONPs display the zeta

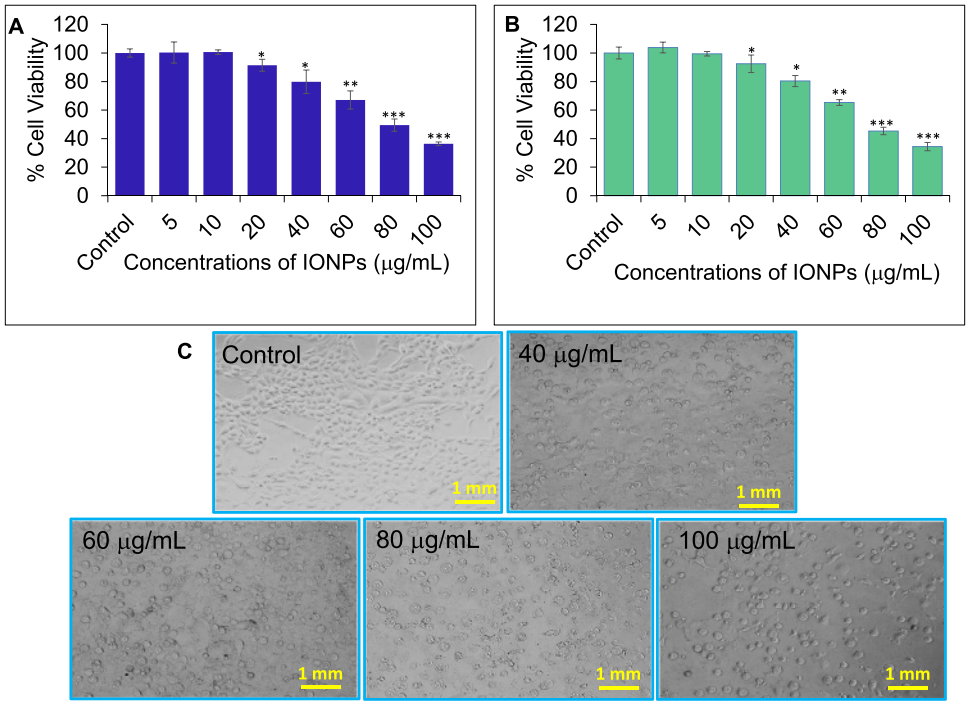

Fig. 5. Cytotoxic effects of IOPNs on HUVECs. Percentage cell viability was assessed by (A) MTT assay, (B) NRU assay. *p < 0.05, * *p < 0.01, and * **p < 0.001 vs control. (C) Morphological changes induced by IOPNs in HUVECs. HUVECs exposed to indicated concentrations of IONPs for 24 h and visualized using phase contrast inverted light microscopy (20 ×).

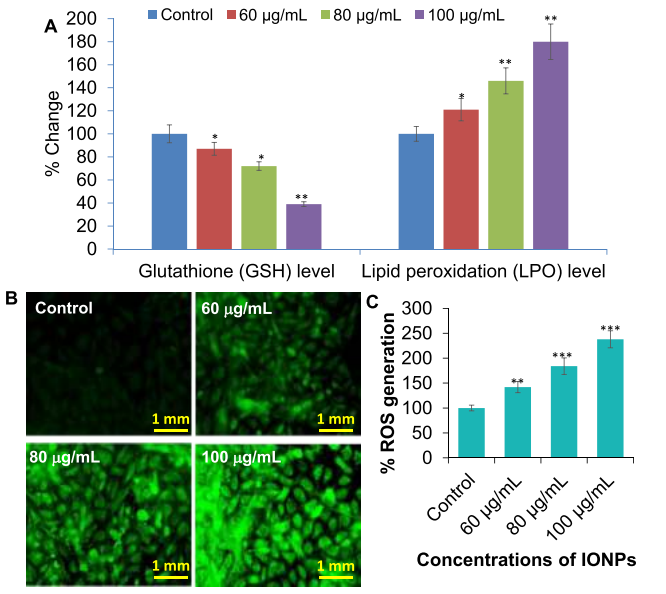

Fig. 6. (A) Oxidative stress measurement by analysis of depletion in glutathione and induction in lipid peroxidation levels in HUVECs exposed to 60–100 μg/mL of IONPs for 24 h. (B) Representative fluorescence images exhibiting ROS generation in HUVECs after the exposure of IONPs (C) Percentage ROS production in HUVECs after the treatment of IONPs for 24 h. ROS generation was measured by DCF-DA staining. *p < 0.05, * *p < 0.01, and * **p < 0.001 vs control.

potential value of − 12.20 mV, which shows that the particles are stable in aqueous suspension. The well characterized IONPs were further evaluated for their cytotoxic potential on HUVECs. We found that IONPs exhibited a dose dependent significant cytotoxic effects towards HUVECs as examined by MTT and NRU assays. Exposure to IONPs at 20 μg/mL and higher concentrations significantly decreases cell viability of HUVECs, while 10 μg/mL and lower concentrations did not produce cytotoxicity. These cytotoxicity data are in agreement with the findings of Kanagesan et al. [39] who has examined the cytotoxic response of IONPs in this concentration range on human cells. The cytotoxic effects of IONPs on mouse embryonic stem cells have also been testified between the concentration range 20–60 μg/mL [40]. In other study, Hilger and colleagues have revealed that iron oxide nanoparticles significantly suppressed the viability of adenocarcinoma cells [41]. A number of researches also reported a dose dependent cytotoxicity of IONPs on different cell types including human fibroblast [42], human lung epithelial cells [43], primary rat hepatocytes [44], and human neuroblastoma cells [45].

Several in vitro reports have described that IONPs induced cytotoxicity through free radical generation and oxidative stress [43,46]. Further to study the role of oxidative stress markers in IONPs induced HUVECs cytotoxicity, glutathione (GSH) depletion and lipid peroxidation (LPO) level were quantified. Our results showed that the GSH level was expressively decreased and LPO level was significantly augmented in a dose dependent way in HUVECs exposed to IONPs for 24 h at 60, 80, and 100 μg/mL concentrations. These findings are in agreement with other reports exhibiting IONPs could induce cell death mediated through oxidative stress by decreasing GSH content and increasing LPO level [43]. Similarly, other researches also established that the cytotoxic effects of IONPs are associated with oxidative stress [47]. ROS are the molecules known for causing the oxidative stress in cellular system [48]. Numerous nanoparticles are known to produce oxidative stress in cultured cells by inducing ROS generation [49]. To explore the mode of cell death induced by IONPs, the HUVECs were stained with DCF-DA dye and ROS production was measured. As elucidated in Fig. 6, a dose dependent significant ROS generation was found in HUVECs treated with IONPs. It is defined that at normal level, ROS is involved in regulating the normal cell functions, but elevated level of ROS generation induces cell death [50]. Our findings are also supported by other investigators who have revealed that excess production of ROS upon IONPs exposure can induce cytotoxicity in various cell types [51]. Numerous reports also suggested that high level of ROS generation upon

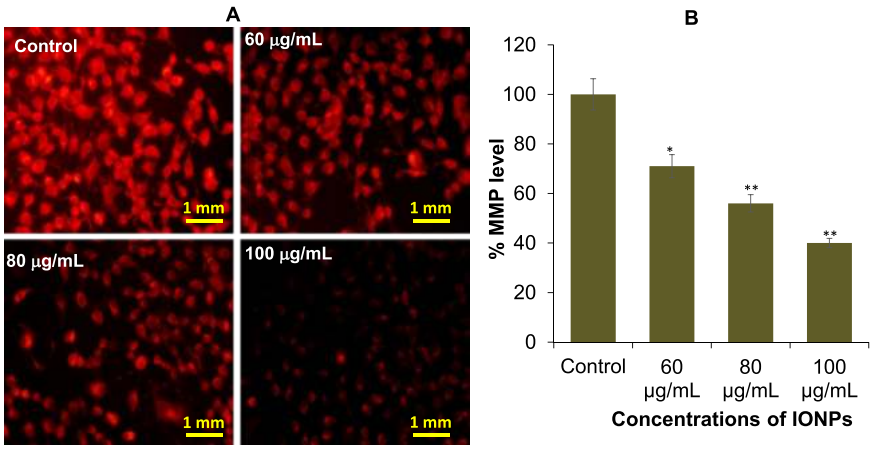

Fig. 7. Measurement of MMP in HUVECs after the exposure of IONPs. HUVECs were treated with IONPs (60, 80, and 100 μg/mL) for 24 h and stained with Rh-123 dye. (A) Representative fluorescence images of HUVECs exhibiting intensity of Rh-123 dye in control and treated cells (B) Graphical representation of percentage loss of MMP in HUVECs after the exposure of IONPs for 24 h. *$p < 0.01$, and * *$p < 0.001$ vs control.

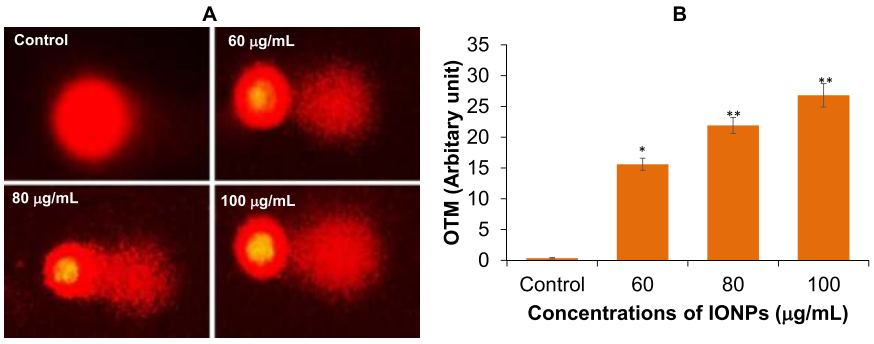

Fig. 8. Effects of IONPs exposure on DNA double strand break in HUVECs. HUVECs were treated with 0, 60, 80, and 100 μg/mL of IONPs for 24 h and DNA damage was measured by comet assay. (A) Representative comet images showing olive tail moment (OTM) as an indicator of DNA damage in control and treated HUVECs. (B) Bar diagram representing the percentage increase of OTM in HUVECs exposed to IONPs.

nanoparticles exposure can damage cells by producing mitochondrial membrane dysfunction [52]. In this study, we also measured the MMP level in HUVECs. We found that the exposure to IONPs reduces the MMP level in HUVECs. As shown in Fig. 7, the fluorescence intensity of Rh-123, a mitochondrial membrane specific cationic dye was decreased dose dependently in IONPs treated HUVCEs. Mitochondrial membrane potential is a sensitive indicator of mitochondrial damage that characterizes an initial incident in mitochondrial cell death pathway [53]. It is essential for balancing the physiological production of ATP by electron transport chain. A substantial loss of MMP causes energy exhaustion and cell death as a result of opening of permeability transition pore complex, accumulated at the inner/outer mitochondrial membrane junction [54]. It is well known that occupational and/or environmental exposure to various nanoparticles provoke constant loss of MMP leading to cell death [55].

ROS generation induced by nanoparticles play a vital role in genotoxicity. Overproduction of ROS is one of the mechanisms of nanotoxicity. The cell death induced by IONPs could be found due to the DNA damage. Consequently, in present investigation, we found that 24 h exposure of IONPs caused a significant DNA damage as detected by a dose dependent increase in the olive tail moment in HUVECs. These results clearly suggested that IONPs have the capability to induce DNA damage in HUVECs. It is reported that excessive free radicals' generation can produce oxidative stress, resulting in cells deteriorating to balance normal physiological functions, thus leads to DNA damage [5]. These ROS can diffuse to the nucleus and damage DNA with double chain breakage formation. Therefore, we assume that the DNA damage occurred in HUVECs is mediated by ROS generation as we observed.

Indeed, it is noteworthy that the pronounced DNA damage induced by IONPs suggests that DNA could be a goal of nanoparticles associated with cell cycle arrest. Further to explore the mechanism by which IONPs induce cell death of HUVECs, we performed cell cycle analysis by flow cytometry. We found that the percentage of SubG1 cell population was dose-dependently increased in HUVECs upon IONPs exposure for 24 h. Our results are consistent with the other studies where cell population at SubG1 phase was significantly increased in IONPs treated cells, confirming the induction of apoptosis by IONPs [56]. Further in order to confirm the role of apoptosis in IONPs induced cell death, the mRNA expression of apoptosis related genes, i.e. p53, bax, caspase-3, caspase-9 and bcl-2 were measured by qRT-PCR. Our data showed that mRNA expression level of proapoptotic p53, bax, caspase-3 and caspase-9 genes was increased and antiapoptotic gene, bcl-2 was downregulated. Numerous studies have also established that these proapoptotic and antiapoptotic genes play an important role in apoptosis and mitochondrial signaling pathway induced by various nanoparticles [34,57]. Consistent with previous studies, our results also suggested that IONPs induced apoptosis in HUVECs depend on mitochondrial mediated apoptotic pathway.

5. Conclusion

Based on the findings of present investigation, we concluded that IONPs are cytotoxic to HUVECs in the concentration range of 20–100 μg/mL. IONPs were also found to induce oxidative stress by increasing LPO and decreasing GSH levels. HUVECs exposed to IONPs was found to increase ROS generation which in turn damaged the MMP.

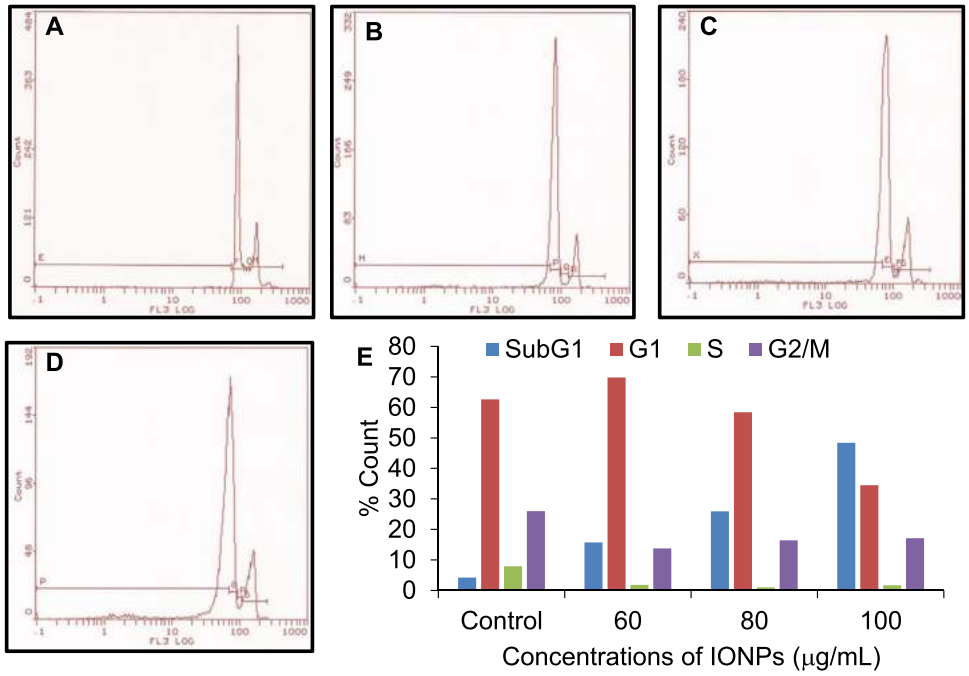

Fig. 9. Cell cycle distribution of HUVECs as analyzed by flow cytometry. Cells exposed to IONPs were stained with PI after fixation. Representative flowcytometric histogram exhibiting cell cycle arrest in (A) Control, (B) 60 μg/mL of IONPs, (C) 80 μg/mL of IONPs, (D) 100 μg/mL of IONPs, and (E) % count in cell population for each phase of cell cycle.

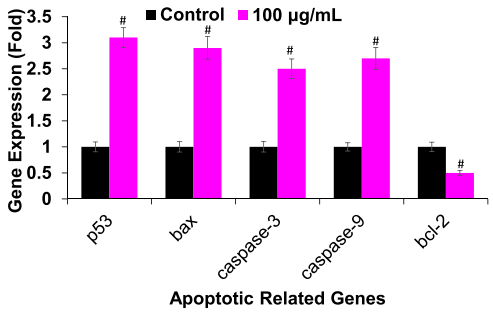

Fig. 10. Expression level of p53, bax, caspase-3, caspase-9, and bcl-2 genes in control and HUVECs treated with 100 μg/mL of IONPs for 24 h. #$p < 0.001$ vs control.

Further IONPs induced DNA damage and SubG1 cell cycle arrest leads to apoptosis in HUVECs. The increased expression of proapoptotic marker genes and decreased expression of antiapoptotic gene clearly revealed that IONPs have the capability to induce apoptosis in HUVECs. Collectively, this in vitro study provides a novel understanding into the mechanism(s) of IONPs induced toxicity and potential hazards linked with human health. Further the risk related to human exposure should be examined under in vivo condition.

CRediT authorship contribution statement

Maqsood A. Siddiqui: Conceptualization, Investigation, Validation, Writing – original draft. **Rizwan Wahab:** Methodology, Investigation. **Quaiser Saquib:** Methodology, Data curation. **Javed Ahmad:** Methodology, Data curation. **Nida N. Farshori:** Data curation, Writing – review & editing. **Ebtesam S. Al-Sheddi:** Methodology, Data curation. **Mai M. Al-Oqail:** Methodology, Data curation. **Shaza M. Al-Massarani:** Formal analysis, Writing – review & editing. **Abdulaziz A. Al-Khedhairy:** Resources, Supervision.

Declaration of Competing Interest

The authors declare that they have no known competing financial interests or personal relationships that could have appeared to influence the work reported in this paper.

Acknowledgement

The authors extend their appreciation to the Deputyship for Research & Innovation, Ministry of Education in Saudi Arabia for funding this research (IFKSURC-1-3204).

References

[1] S. Malik, K. Muhammad, Y. Waheed, Nanotechnology: a revolution in modern industry, Molecules 28 (2023) 661.
[2] N. Joudeh, D. Linke, Nanoparticle classification, physicochemical properties, characterization, and applications: a comprehensive review for biologists, J. Nanobiotechnol. 20 (2022) 262.
[3] A. Yusuf, A.R. Almotairy, H. Henidi, O.Y. Alshehri, M.S. Aldughaim, Nanoparticles as drug delivery systems: a review of the implication of nanoparticles' physicochemical properties on responses in biological systems, Polymers 15 (2023) 1596.
[4] T.M. Joseph, D. Kar Mahapatra, A. Esmaeili, Ł. Piszczyk, M.S. Hasanin, M. Kattali, J. Haponiuk, S. Thomas, Nanoparticles: Taking a unique position in medicine, Nanomaterials 13 (2023) 574.
[5] P.P. Fu, Q. Xia, H.M. Hwang, P.C. Ray, H. Yu, Mechanisms of nanotoxicity: generation of reactive oxygen species, J. Food Drug Anal. 22 (2014) 64–75.
[6] R. Gupta, H. Xie, Nanoparticles in daily life: applications, toxicity and regulations, J. Environ. Pathol. Toxicol. Oncol. 37 (2018) 209–230.
[7] A. Nel, T. Xia, L. Madler, N. Li, Toxic potential of materials at the nanolevel, Science 311 (2006) 622–627.
[8] T. Xia, M. Kovochich, M. Liong, L. Madler, B. Gilbert, H. Shi, J.I. Yeh, J.I. Zink, A. E. Nel, Comparison of the mechanism of toxicity of zinc oxide and cerium oxide nanoparticles based on dissolution and oxidative stress properties, ACS Nano 2 (2008) 2121–2134.
[9] H. Bahadar, F. Maqbool, K. Niaz, M. Abdollahi, Toxicity of nanoparticles and an overview of current experimental models, Iran. Biomed. J. 20 (2016) 1–11.
[10] A. Weir, P. Westerhoff, L. Fabricius, K. Hristovski, N. Von Goetz, Titanium dioxide nanoparticles in food and personal care products, Environ. Sci. Technol. 46 (2012) 2242–2250.
[11] R.J. Aitken, M.Q. Chaudhry, A.B. Boxall, M. Hull, Manufacture and use of nanomaterials: current status in the UK and global trends, Occup. Med 56 (2006) 300–306.

[12] C. Egbuna, V.K. Parmar, J. Jeevanandam, S.M. Ezzat, K.C. Patrick-Iwuanyanwu, C. O. Adetunji, J. Khan, E.N. Onyeike, C.Z. Uche, M. Akram, M.S. Ibrahim, Toxicity of nanoparticles in biomedical application: nanotoxicology, J. Toxicol. 2021 (2021) 9954443.
[13] S. Raj, D. Kumar, Biochemical toxicology: heavy metals and nanomaterials, Biochem. Toxicol. Heavy Met. Nanomater 139 (2020) 10.5772.
[14] A. Adamcakova-Dodd, P.S. Thorne, V.H. Grassian, In vivo toxicity studies of metal and metal oxide nanoparticles, Handb. Syst. Toxicol. (2011) 803–834.
[15] S. Kheiri, X. Liu, M. Thompson, Nanoparticles at biointerfaces: antibacterial activity and nanotoxicology, Colloids Surf. B Biointerfaces 184 (2019), 110550.
[16] Y.W. Huang, M. Cambre M, H.J. Lee, The toxicity of nanoparticles depends on multiple molecular and physicochemical mechanisms, Inter. J. Mol. Sci. 18 (2017) 2702.
[17] P. Khanna, C. Ong, B.H. Bay, G.H. Baeg, Nanotoxicity: an interplay of oxidative stress, inflammation and cell death, Nanomaterials 5 (2015) 1163–1180.
[18] Y. Min, G.G. Suminda, Y. Heo, M. Kim, M. Ghosh, Y.O. Son, Metal-based nanoparticles and their relevant consequences on cytotoxicity cascade and induced oxidative stress, Antioxidants 12 (2023) 703.
[19] L.S. Arias, J.P. Pessan, A.P. Vieira, T.M. Lima, A.C. Delbem, D.R. Monteiro, Iron oxide nanoparticles for biomedical applications: A perspective on synthesis, drugs, antimicrobial activity, and toxicity, Antibiotics 7 (2018) 46.
[20] V. Valdiglesias, N. Fernández-Bertólez, G. Kiliç, C. Costa, S. Costa, S. Fraga, M. J. Bessa, E. Pásaro, J.P. Teixeira, B. Laffon, Are iron oxide nanoparticles safe? Current knowledge and future perspectives, J. Trace Elem. Med. Biol. 38 (2016) 53–63.
[21] J.H. Lee, J.E. Ju, B.I. Kim, P.J. Pak, E.K. Choi, H.S. Lee, N. Chung, Rod-shaped iron oxide nanoparticles are more toxic than sphere-shaped nanoparticles to murine macrophage cells, Environ. Toxicol. Chem. 33 (2014) 2759–2766.
[22] S.C. Hong, J.H. Lee, J. Lee, H.Y. Kim, J.Y. Park, J. Cho, J. Lee, D.W. Han, Subtle cytotoxicity and genotoxicity differences in superparamagnetic iron oxide nanoparticles coated with various functional groups, Int. J. Nanomed. 6 (2011) 3219–3231.
[23] N. Singh, G.J. Jenkins, R. Asadi, S.H. Doak, Potential toxicity of superparamagnetic iron oxide nanoparticles (SPION), Nano Rev. 1 (2010) 5358.
[24] V. Valdiglesias, G. Kiliç, C. Costa, N. Fernández-Bertólez, E. Pásaro, J.P. Teixeira, B. Laffon, Effects of iron oxide nanoparticles: cytotoxicity, genotoxicity, developmental toxicity, and neurotoxicity, Environ. Mol. Mutagen. 56 (2015) 125–148.
[25] U.S. Gaharwar, R. Meena, P. Rajamani, Iron oxide nanoparticles induced cytotoxicity, oxidative stress and DNA damage in lymphocytes, J. Appl. Toxicol. 37 (2017) 1232–1244.
[26] K. Buyukhatipoglu, A.M. Clyne, Superparamagnetic iron oxide nanoparticles change endothelial cell morphology and mechanics via reactive oxygen species formation, J. Biomed. Mater. Res. A 96 (2011) 186–195.
[27] T. Wen, L. Du, B. Chen, D. Yan, A. Yang, J. Liu, N. Gu, J. Meng, H. Xu, Iron oxide nanoparticles induce reversible endothelial-to-mesenchymal transition in vascular endothelial cells at acutely non-cytotoxic concentrations, Part. Fibre Toxicol. 16 (2019) 30.
[28] R. Wahab, F. Khan, A.A. Al-Khedhairy, Hematite iron oxide nanoparticles: apoptosis of myoblast cancer cells and their arithmetical assessment, RSC Adv. 8 (2018) 24750–24759.
[29] R. Wahab, F. Khan, N. Kaushik, N.K. Kaushik, L.N. Nguyen, E.H. Choi, M. A. Siddiqui, N.N. Farshori, Q. Saquib, J. Ahmad, A.A. Al-Khedhairy, L-cysteine embedded core-shell ZnO microspheres composed of nanoclusters enhances anticancer activity against liver and breast cancer cells, Toxicol. Vitr. 85 (2022), 105460.
[30] M.A. Siddiqui, Q. Saquib, M. Ahamed, N.N. Farshori, J. Ahmad, R. Wahab, S. T. Khan, H.A. Alhadlaq, J. Musarrat, A.A. Al-Khedhairy, A.B. Pant, Molybdenum nanoparticles-induced cytotoxicity, oxidative stress, G2/M arrest, and DNA damage in mouse skin fibroblast cells (L929), Colloids Surf B Bio Interfaces 125 (2015) 73–81.
[31] M.A. Siddiqui, G. Singh, M.P. Kashyap, V.K. Khanna, S. Yadav, D. Chandra, A. B. Pant, Influence of cytotoxic doses of 4-hydroxynonenal on selected neurotransmitter receptors in PC-12 cells, Toxicol. Vitr. 22 (2008) 1681–1688.
[32] D. Chandra, K.V. Ramana, L. Wang, B.N. Christensen, A. Bhatnagar, S. K. Srivastava, Inhibition of fiber cell globulization and hyperglycemia-induced lens opacification by aminopeptidase inhibitor bestatin, Investig. Ophthalmol. Vis. Sci. 43 (2002) 2285–2292.
[33] J.A. Buege, S.D. Aust, Microsomal lipid peroxidation, Methods Enzymol. 52 (1978) 302–310.
[34] M.A. Siddiqui, H.A. Alhadlaq, J. Ahmad, A.A. Al-Khedhairy, J. Musarrat, M. Ahamed, Copper oxide nanoparticles induced mitochondria mediated apoptosis in human hepatocarcinoma cells, PLoS One 8 (2013), e69534.
[35] Q. Saquib, A.A. Al-Khedhairy, M.A. Siddiqui, F.M. Abou-Tarboush, A. Azam, J. Musarrat, Titanium dioxide nanoparticles induced cytotoxicity, oxidative stress and DNA damage in human amnion epithelial (WISH) cells, Toxicol. Vitr. 26 (2012) 351–361.
[36] J. Ahmad, R. Wahab, M.A. Siddiqui, Q. Saquib, N. Ahmad, A.A. Al-Khedhairy, Strontium-doped nickel oxide nanoparticles: synthesis, characterization, and cytotoxicity study in human lung cancer A549 cells, Biol. Trace Elem. Res. 200 (2022) 1598–1607.
[37] J. Sarkar, S. Das, S. Aich, P. Bhattacharyya, K. Acharya, Antiviral potential of nanoparticles for the treatment of Coronavirus infections, J. Trace Elem. Med. Biol. 72 (2022), 126977.
[38] N. Malhotra, J.S. Lee, R.A. Liman, J.M. Ruallo, O.B. Villaflores, T.R. Ger, C. D. Hsiao, Potential toxicity of iron oxide magnetic nanoparticles: a review, Molecules 25 (2020) 3159.
[39] S. Kanagesan, M. Hashim, S. Tamilselvan, N.B. Alitheen, I. Ismail, A. Hajalilou, K. Ahsanul, Synthesis, characterization, and cytotoxicity of iron oxide nanoparticles, Adv. Mater. Sci. Eng. 2013 (2013), 710432.
[40] H. Mohseni Kouchesfehani, S. Kiani, A.A. Rostami, R. Fakheri, Cytotoxic effect of iron oxide nanoparticles on mouse embryonic stem cells by MTT assay, Iran, J. Toxicol. 7 (2013) 849–853.
[41] I. Hilger, S. Frühauf, W. Linß, R. Hiergeist, W. Andrä, R. Hergt, W.A. Kaiser, Cytotoxicity of selected magnetic fluids on human adenocarcinoma cells, J. Magn. Magn. Mater. 261 (2003) 7–12.
[42] M.A. Abakumov, A.S. Semkina, A.S. Skorikov, D.A. Vishnevskiy, A.V. Ivanova, E. Mironova, G.A. Davydova, A.G. Majouga, V.P. Chekhonin, Toxicity of iron oxide nanoparticles: size and coating effects, J. Biochem. Mol. Toxicol. 32 (2018), e22225.
[43] S. Dwivedi, M.A. Siddiqui, N.N. Farshori, M. Ahamed, J. Musarrat, A.A. Al-Khedhairy, Synthesis, characterization and toxicological evaluation of iron oxide nanoparticles in human lung alveolar epithelial cells, Colloids Surf. B Biointerfaces 122 (2014) 209–215.
[44] K. Gokduman, F. Bestepe, L. Li, M.L. Yarmush, O.B. Usta, Dose-, treatment-and time-dependent toxicity of superparamagnetic iron oxide nanoparticles on primary rat hepatocytes, Nanomedicine 13 (2018) 1267–1284.
[45] C. Hoskins, A. Cuschieri, L. Wang, The cytotoxicity of polycationic iron oxide nanoparticles: common endpoint assays and alternative approaches for improved understanding of cellular response mechanism, J. Nanobiotechnol. 10 (2012) 15.
[46] M. Ahamed, H.A. Alhadlaq, M.M. Khan, M.J. Akhtar, Selective killing of cancer cells by iron oxide nanoparticles mediated through reactive oxygen species via p53 pathway, J. Nanopart. Res. 15 (2013) 1225.
[47] M. Horie, Y. Tabei, Role of oxidative stress in nanoparticles toxicity, Free Radic. Res. 55 (2021) 331–342.
[48] M.L. Circu, T.Y. Aw, Reactive oxygen species, cellular redox systems, and apoptosis, Free Radic. Biol. Med. 48 (2010) 749–762.
[49] J. Čapek, T. Roušar, Detection of oxidative stress induced by nanomaterials in cells—the roles of reactive oxygen species and glutathione, Molecules 26 (2021) 4710.
[50] C. Zhang, X. Wang, J. Du, Z. Gu, Y. Zhao, Reactive oxygen species-regulating strategies based on nanomaterials for disease treatment, Adv. Sci. 8 (2021) 2002797.
[51] M.O. Ansari, N. Parveen, M.F. Ahmad, A.L. Wani, S. Afrin, Y. Rahman, S. Jameel, Y. A. Khan, H.R. Siddique, M. Tabish, G.G. Shadab, Evaluation of DNA interaction, genotoxicity and oxidative stress induced by iron oxide nanoparticles both in vitroand in vivo: attenuation by thymoquinone, Sci. Rep. 9 (2019) 6912.
[52] A. Manke, L. Wang, Y. Rojanasakul, Mechanisms of nanoparticle-induced oxidative stress and toxicity, BioMed. Res. Int. 2013 (2013), 942916.
[53] S. Hussain, Measurement of nanoparticle-induced mitochondrial membrane potential alterations, Methods Mol. Biol. 2019 (1894) 123–131.
[54] M. Bonora, M.R. Wieckowski, C. Chinopoulos, O. Kepp, G. Kroemer, L. Galluzzi, P. Pinton, Molecular mechanisms of cell death: central implication of ATP synthase in mitochondrial permeability transition, Oncogene 34 (2015) 1475–1486.
[55] L. Patrón-Romero, P.A. Luque-Morales, V. Loera-Castañeda, I. Lares-Asseff, M.Á. Leal-Ávila, J.A. Alvelais-Palacios, I. Plasencia-López, H. Almanza-Reyes, Mitochondrial dysfunction induced by zinc oxide nanoparticles, Crystals 12 (2022) 1089.
[56] F. Namvar, H.S. Rahman, R. Mohamad, J. Baharara, M. Mahdavi, E. Amini, M. S. Chartrand, S.K. Yeap, Cytotoxic effect of magnetic iron oxide nanoparticles synthesized via seaweed aqueous extract, Int. J. Nanomed. 9 (2014) 2479–2488.
[57] L.N. Al-Harbi, G.M. Al-Shammari, P. Subash-Babu, M.A. Mohammed, R. A. Alkreadees, A.E. Yagoub, Cinchona officinalis phytochemicals-loaded iron oxide nanoparticles induce cytotoxicity and stimulate apoptosis in MCF-7 human breast cancer cells, Nanomaterials 12 (2022) 3393.